

# Systematic Study of New Rare Earth Element–Iron–Antimony Skutterudites Synthesized Using Multilayer Precursors

Marc D. Hornbostel, Edward J. Hyer, Julie H. Edvalson, and David C. Johnson\*

Department of Chemistry and Materials Science Institute, University of Oregon, Eugene, Oregon 97403

Received February 27, 1997<sup>⊗</sup>

We have synthesized a series of stable and metastable rare earth element–iron antimonides, controlling both composition and structure using multilayer reactants. The stable rare earth iron element antimonides have the filled skutterudite structure (LaFe<sub>4</sub>P<sub>12</sub>) with a stoichiometry of 1 for the rare earth element. The metastable rare earth element–iron antimonides could be prepared with the entire sequence of rare earth elements. The lattice parameters of these metastable compounds were always larger than those of the corresponding more stable analog, and the occupancy of the rare earth element cation was found to be less than 1. Reitveld analysis of Lu<sub>1-x</sub>Fe<sub>4</sub>Sb<sub>12</sub> suggests that the late rare earth element compounds have a new distorted filled skutterudite structure. Structural trends are discussed in terms of their potential use as thermoelectric materials.

## Introduction

The iron–cobalt antimonides with the filled skutterudite structure were recently promoted as possible new thermoelectric materials.<sup>1</sup> These materials are structurally related to the cubic mineral skutterudite (CoAs<sub>3</sub>).<sup>2</sup> Compounds with the CoAs<sub>3</sub> structure can also be synthesized with the other pnictogens as well as isoelectronic mixtures of group 4 and 6 elements.<sup>3</sup> When iron is substituted for cobalt, the structure is electron deficient but can be stabilized by incorporating an electropositive element into an interstitial site, producing a compound with the “filled skutterudite” (LaFe<sub>4</sub>P<sub>12</sub>) structure type.<sup>4</sup>

The antimonides with this filled structure are promising thermoelectric materials because of an unusual structural property. They can be formed with cations which are significantly smaller than their interstitial site. As a result, these ions have unusually large thermal vibration amplitudes and therefore are strong phonon scatters. The electrical conduction, however, occurs in the transition metal and antimony framework and is not affected by the motion of the cations. The result is a suppression of the phonon thermal conductivity without adverse effects on the electrical properties.<sup>1</sup> This suppression is a large effect, with a reduction in lattice thermal conductivity by a factor of 10–.<sup>5</sup>

This suppression of the phonon thermal conductivity is important, since thermoelectric materials are evaluated for performance on the basis of the magnitude of their figure of merit

$$Z = S^2\sigma/\kappa$$

where  $S$  is the Seebeck coefficient,  $\sigma$  is the electrical conductivity, and  $\kappa$  is the total thermal conductivity.<sup>6</sup> The total thermal conductivity is the sum of the lattice and electronic contributions. Since the dimensions of  $Z$  are inverse temperature, the dimensionless figure of merit  $ZT$ , where  $T$  is the absolute

temperature, is often used. A reduction in the lattice thermal conductivity increases  $Z$  directly and also increases it in a way not obvious by the formula above. Since the losses in maintaining the thermal gradient are reduced by a reduction in lattice thermal conductivity, less current needs to flow through the device. A semiconductor with a smaller carrier concentration can then be used. Since the Seebeck coefficient increases with decreasing carrier concentration, this results in an increased Seebeck coefficient and a further enhanced figure of merit.<sup>7</sup>

The electronic contribution to the thermal conductivity and the electrical conductivity are, of course, related. The Wiedemann–Franz law states that the ratio of these quantities is proportional to temperature. The proportionality factor, called the Lorenz number ( $L$ ), depends only on fundamental constants and has the value of  $2.45 \times 10^{-8} \text{ W } \Omega/\text{K}^2$ . In the limit of negligible lattice thermal conductivity compared with the magnitude of the electronic contribution, the dimensionless figure of merit,  $ZT$  reduces to

$$ZT = S^2/L$$

The magnitude of the figure of merit is then intimately tied to the magnitude of the cooling power required. An increase in required cooling power requires an increase in the carrier concentration, which reduces the Seebeck coefficient. One would like to vary the electropositive cation in the structure to find the cation with the minimal lattice thermal conductivity. The electrical properties could then be optimized by varying the iron to cobalt ratio (or replacing antimony with germanium or tin) to maximize the Seebeck coefficient independently of the lattice thermal conductivity. A Seebeck coefficient of several hundred microvolts per kelvin would result in a commercially useful material if the thermal conductivity was reduced to the theoretical minimum value.

This “rattling” cation structural feature is unusual in solid state compounds because such size mismatches cause a reduction in the Madelung energy, which is important for the stability of the crystalline structure. A compound in which an ion is located in a larger hole is generally unstable. However, because the thermoelectric properties are improved by this size mismatch, it is desirable to increase this mismatch as much as possible. The lanthanide sequence provides an opportunity to systemati-

\* Corresponding author.

⊗ Abstract published in *Advance ACS Abstracts*, August 15, 1997.

(1) Sales, B. C.; Mandrus, D.; Williams, R. K. *Science* **1996**, *272*, 1325.  
 (2) Braun, D. J.; Jeitschko, W. *J. Less-Common Met.* **1980**, *72*, 147.  
 (3) Kjekshus, A.; Rakke, T. *Acta Chem. Scand., Ser. A* **1974**, *28*, 99.  
 (4) Jeitschko, W.; Braun, D. *Acta Crystallogr.* **1977**, *B33*, 3401.  
 (5) Nolas, G. S.; Slack, G. A.; Morelli, D. T.; Tritt, T. M.; Ehrlich, A. C. *J. Appl. Phys.* **1996**, *79*, 4002.  
 (6) Wood, C. *Rep. Prog. Phys.* **1988**, *51*, 459.

(7) Mahan, G.; Sales, B.; Sharp, J. *Phys. Today* **1997**, *50*, 42.

**Table 1.** Summary of Samples Used in This Study<sup>a</sup>

| sample | intended thickness (Å) |     |    | measd <i>d</i> (Å) | compn (Sb 12) |      |
|--------|------------------------|-----|----|--------------------|---------------|------|
|        | Ln                     | Fe  | Sb |                    | Ln            | Fe   |
| La     | 1.5                    | 1.9 | 15 | 21.4               | 0.81          | 4.17 |
| Ce     | 1.2                    | 1.6 | 15 | 20.4               | 1.33          | 3.90 |
| Pr     | 1.2                    | 1.6 | 15 | 21.0               | 0.92          | 4.00 |
| Nd     | 1.2                    | 1.6 | 15 | 20.6               | 1.20          | 4.13 |
| Sm     | 1.2                    | 1.6 | 15 | 19.2               | 0.93          | 3.27 |
| Eu     | 1.7                    | 1.6 | 15 | 21.0               | 0.94          | 3.40 |
| Gd     | 1.2                    | 1.6 | 15 | 20.0               | 1.09          | 4.38 |
| Tb     | 1.2                    | 1.6 | 15 | 20.3               | 0.87          | 3.62 |
| Dy     | 1.0                    | 1.6 | 15 | 19.1               | 0.60          | 3.60 |
| Ho     | 1.1                    | 1.6 | 15 | 19.7               | 0.97          | 3.64 |
| Er     | 1.1                    | 1.6 | 15 | 19.9               | ~0.9          | ~3.8 |
| Tm     | 1.1                    | 1.6 | 15 | 19.0               | 0.77          | 3.74 |
| Yb     | 1.4                    | 1.6 | 15 | 19.2               | 0.85          | 3.89 |
| Lu     | 1.0                    | 1.6 | 15 | 20.0               | 0.73          | 3.76 |

<sup>a</sup> Multilayer repeat thicknesses were measured by low-angle X-ray diffraction to the nearest 0.1 Å. Compositions were determined by an electron microprobe to approximately 1%.

cally study the effects of the cation radius on the structural and the physical properties of the filled skutterudites. With the exception of europium and ytterbium, the lanthanides are all expected to be isoelectronic in these compounds but to have ionic radii which decrease monotonically from lanthanum to lutetium.<sup>8</sup>

In order to study these structural and electronic trends, it is necessary to synthesize the entire sequence of LnFe<sub>4</sub>Sb<sub>12</sub>. The majority of these compounds are not thermodynamically stable, and so we used the multilayer precursor method, which is capable of producing metastable compounds at low temperatures.<sup>9</sup> In this method, the elements to be reacted are vacuum-deposited to form a thin-film multilayer structure. The multilayer repeat distance is kept extremely small so that the elements need only diffuse a short distance to react. If this length is short enough, the elements will mix before any crystalline compounds can nucleate.<sup>10</sup> The result is a kinetically stable, amorphous reaction intermediate. From there, compound formation is determined by nucleation kinetics and is no longer diffusion limited.<sup>11</sup> The reaction kinetics can be controlled to produce a particular compound by the average composition<sup>12</sup> or possibly by seeding, either with an isostructural compound or with an epitaxially matched substrate.<sup>13</sup>

We have prepared Ln–Fe–Sb multilayer films with every lanthanide except promethium (because of its radioactivity). From these multilayer films we were able to produce the entire series of low-temperature, metastable, filled skutterudites. Here we report the structural trends observed in these compounds, which can be used to guide the search for optimal thermoelectric materials.

## Experimental Section

The multilayer samples were prepared in a high-vacuum evaporation system which has been described in detail elsewhere.<sup>14</sup> Briefly, the elements were sequentially deposited under high vacuum (approximately  $5 \times 10^{-7}$  Torr) under the control of a personal computer. The elements were deposited from electron beam evaporation sources at a rate of

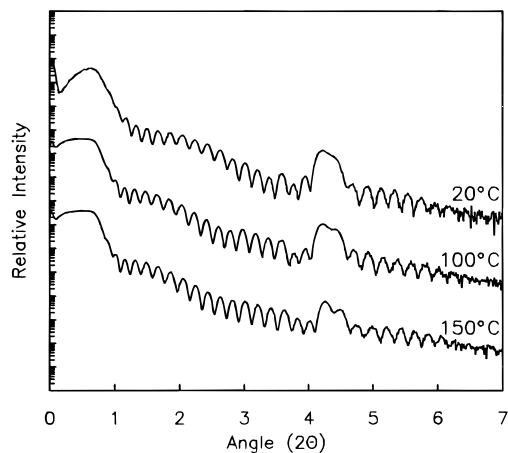


**Figure 1.** Low-angle diffraction of a Eu–Fe–Sb multilayer on silicon. Top curve is from the as-deposited sample. Lower two curves are after successive 1 h annealings at the indicated temperature. Each curve is offset by a factor of 1000 for clarity.

0.5 Å/s. Each source was independently monitored by quartz crystal thickness monitors. The thickness of each elemental layer was controlled to the nearest angstrom. The elemental compositions of the samples were found to be repeatable to within about 5%. The films were simultaneously deposited on silicon and photoresist-coated silicon wafers. The silicon substrates were used for low-angle diffraction studies. The coated substrates were used to allow the sample to be removed from the substrate by soaking in acetone and collecting with PTFE filters.

Low-angle X-ray diffraction was used to characterize the multilayer periodicity and to study the interdiffusion of the elements. High-angle X-ray diffraction was used to identify crystalline compounds. The average composition of the multilayer films was determined by electron microprobe analysis using an energy-dispersive X-ray detector.

Samples were annealed under a nitrogen atmosphere. Substrate-free samples were annealed in a differential scanning calorimeter. Measured exotherms were correlated with X-ray results to identify and track the interdiffusion of the elements and the crystallization of any compounds.

## Results and Discussion

Table 1 contains a summary of the samples prepared in the course of this research. The intended thicknesses are listed along with the measured repeat distances obtained from low-angle diffraction measurements. The actual thickness is systematically greater than the sum of the intended thicknesses. This is, in part, due to the multilayer having a lower density than the bulk elements. However, the thickness monitors primarily measure deposited mass so density variations do not significantly affect the sample composition. The iron to antimony ratio was calibrated on the basis of a series of La–Fe–Sb samples and was chosen to be slightly iron poor to suppress the formation of FeSb<sub>2</sub>. The intended thickness of the rare earth element component was calculated to give a stoichiometric composition based on the density of the bulk rare earth metal. The composition determined by microprobe analysis shows an approximately 10% variation from sample to sample, which is sufficiently precise to produce the desired compounds in this system.

An example of a low-angle diffraction pattern from a Eu–Fe–Sb sample is shown in Figure 1. The uppermost pattern is from the as-deposited multilayer sample. The other patterns are from consecutive, 1 h annealing steps at the indicated temperatures. The feature below 1° in all of the patterns is the specular reflection of the X-ray beam from the top surface of the sample. The smaller peaks are due to interference between reflections from the top and bottom surfaces of the film. From

- (8) Shannon, R. D. *Acta Crystallogr.* **1976**, A32, 751.  
 (9) Novet, T.; Johnson, D. C. *J. Am. Chem. Soc.* **1991**, 113, 3398.  
 (10) Fister, L.; Johnson, D. C. *J. Am. Chem. Soc.* **1992**, 114, 4639.  
 (11) Fukuto, M.; Hornbostel, M. D.; Johnson, D. C. *J. Am. Chem. Soc.* **1994**, 116, 9136.  
 (12) Oyelaran, O.; Novet, T.; Johnson, C. D.; Johnson, D. C. *J. Am. Chem. Soc.* **1996**, 118, 2422.  
 (13) Noh, M.; Johnson, C. D.; Hornbostel, M. D.; Thiel, J.; Johnson, D. C. *Chem. Mater.* **1996**, 8, 1625.  
 (14) Fister, L.; Li, X. M.; Novet, T.; McConnell, J.; Johnson, D. C. *J. Vac. Sci. Technol., A* **1993**, 11, 3014.

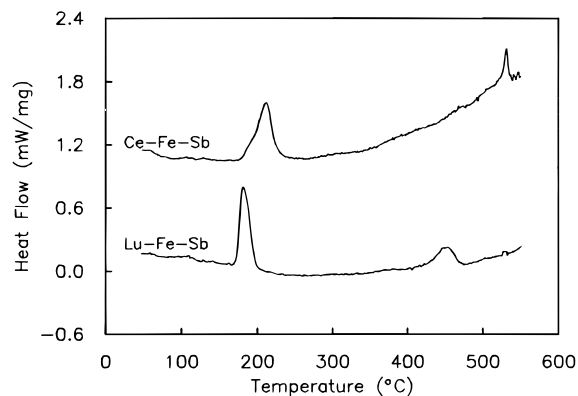


**Figure 2.** Differential scanning calorimetry data of an early and a late rare earth element–iron–antimony multilayer sample. Each shows two irreversible exotherms from the formation and decomposition of a metastable skutterudite. Upper curve was offset by 1 mW/mg for clarity.

these, the film thicknesses can be determined. For the sample shown, the total film thickness is 406 Å. In addition, there is a gradual modulation of the intensity of these peaks due to a surface oxide layer. This oxide is approximately 30 Å thick before annealing and 50 Å thick after the first annealing. No further oxide growth is observed after the second annealing step. These samples were stored in air, and we suspect that the oxide formation most likely occurred during storage rather than during the annealing, which was done under a nitrogen atmosphere. The large peak at 4.2° is the first-order Bragg reflection from the periodic multilayer structure. The position of this peak corresponds to a thickness of 21 Å for the repeating unit containing elemental layers of Eu, Fe, and Sb. Higher order peaks are not observed, indicating that the elements are sufficiently intermixed on deposition that the electron density varies in a sinusoidal fashion, with no higher order Fourier components. This implies the composition profile is also approximately sinusoidal. The multilayer diffraction peak is seen to decrease in intensity, particularly after the 150 °C annealing. This shows that significant diffusion of the elements occurs in the 100–200 °C temperature range.<sup>15</sup> The short diffusion distances built into the multilayer sample allow the elements to mix at a sufficiently low temperature (200 °C in this case) that the nucleation kinetics can control the formation of crystalline products.<sup>9</sup>

Calorimetry data for cerium and lutetium samples are shown in Figure 2. The data are strikingly similar for these two samples, each having two irreversible exotherms. This is surprising because the early rare earth elements form stable iron–antimony skutterudites while the later rare earth elements do not. Diffraction data, shown in Figure 3, were collected to determine the structural changes occurring during each of these transitions. Diffraction data taken after heating past the first exotherm of both samples show the formation of the cubic skutterudite structure. The unit cell length calculated for the Ce–Fe–Sb sample, however, is significantly larger than the reported value for the compound  $\text{CeFe}_4\text{Sb}_{12}$ .<sup>2</sup> The large lattice parameter is consistent with the low-temperature crystallization of the lanthanum analog, where structural refinement indicated a partial occupancy of the rare earth metal cation in the large lattice parameter structure.<sup>16</sup> This result suggests that the low-temperature Ce–Fe–Sb compound also has a partial occupancy of the rare earth metal cation.

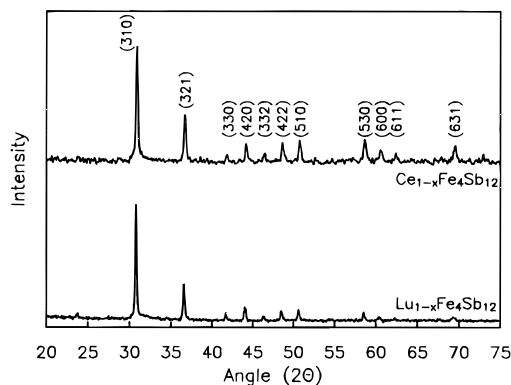


**Figure 3.** X-ray powder patterns of metastable  $\text{Ce}_{1-x}\text{Fe}_4\text{Sb}_{12}$  and  $\text{Lu}_{1-x}\text{Fe}_4\text{Sb}_{12}$ . Skutterudite peaks are indexed as shown.

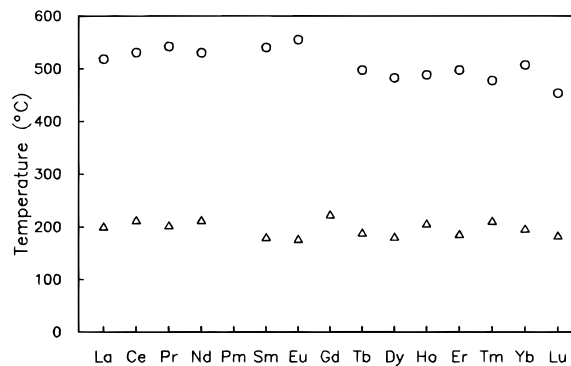


**Figure 4.** Formation (triangles) and decomposition (circles) temperatures of each  $\text{Lu}_{1-x}\text{Fe}_4\text{Sb}_{12}$ . The promethium compound was not studied because of its radioactivity. The  $\text{Gd}_{1-x}\text{Fe}_4\text{Sb}_{12}$  decomposition exotherm was too weak to be observed.

Diffraction data collected after heating past the second exotherm indicate that both samples contain several compounds. In the cerium sample, the distribution of compounds is consistent with the reported high-temperature synthesis of  $\text{CeFe}_4\text{Sb}_{12}$ .<sup>2</sup> This sample contained the stoichiometric  $\text{CeFe}_4\text{Sb}_{12}$ , as determined by the smaller unit cell *a* axis, cerium, antimony, and  $\text{FeSb}_2$ . This phase separation from the single phase  $\text{Ce}_{1-x}\text{Fe}_4\text{Sb}_{12}$  is exothermic and irreversible, which indicates that this low-temperature, partially filled skutterudite is metastable with respect to a mixture of elements, binary compounds, and the stoichiometric  $\text{CeFe}_4\text{Sb}_{12}$ . In contrast, no skutterudite was observed in the lutetium sample after heating past its second exotherm, confirming that while  $\text{CeFe}_4\text{Sb}_{12}$  is stable,  $\text{LuFe}_4\text{Sb}_{12}$  is not.

The calorimetry data for the entire rare earth element sequence are summarized in Figure 4, which shows the formation and decomposition temperatures of metastable, partially filled skutterudites. Every sample had an exotherm near 200 °C, which corresponded to the formation of a filled skutterudite compound. The low temperature of this exotherm (just above the temperature required to interdiffuse the elements) indicates the nucleation of the skutterudite structure is particularly facile. The lack of any variation among these compounds indicates that the nucleation and growth of this structure are independent of the cation. This can be understood by considering the skutterudite structure as a simple corner-sharing network of  $[\text{FeSb}_6]$  octahedra. The iron can be expected to be octahedrally coordinated even in the amorphous mixture, because of the favorable local bonding arrangement. From there, only small rearrangements of the  $[\text{FeSb}_6]$  octahedra are required to form the desired structure. The activation energy for this rearrangement is less than that of forming the more stable mixture of

(15) Novet, T.; McConnell, J. M.; Johnson, D. C. *Chem. Mater.* **1992**, *4*, 473.

(16) Hornbostel, M. D.; Hyer, E. J.; Thiel, J.; Johnson, D. C. *J. Am. Chem. Soc.* **1997**, *119*, 2665.

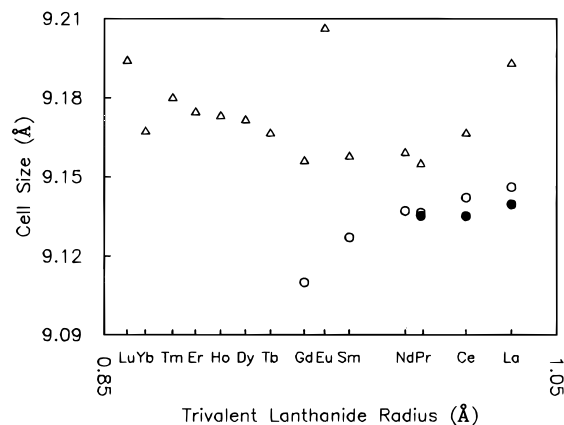


**Figure 5.** Cubic unit cell  $a$  axis length for low-temperature (triangles) and high-temperature (open circles) skutterudites as a function of the ionic radii of the trivalent cations (from ref 8). Data for previously reported compounds are also shown for comparison (filled circles).<sup>2</sup>

compounds because this disproportionation requires long-range diffusion of the elements.

The low-temperature, partially filled skutterudites all decomposed upon heating to 550 °C into a mixture of phases. As shown in Figure 4, a decomposition exotherm was observed for every sample except the gadolinium sample, where the decomposition rate was probably too slow to produce a heat signal in the scanning calorimeter. The La, Pr, Nd, Sm, and Gd samples all contained the stoichiometric filled skutterudite after heating to 550 °C, although the gadolinium sample contained only trace quantities of this high-temperature skutterudite.

To understand the change in stability of the low- and high-temperature skutterudites across the rare earth element sequence, we refined the lattice parameters of all the skutterudite compounds formed in this study. Naively, one expects a gradual, steady decrease in the lattice parameters due to the decrease in size of the rare earth metal cations as a result of the lanthanide contraction. Since the host matrix is not very oxidizing, europium and ytterbium are expected to be formally divalent, as observed, for example, in ternary selenides.<sup>17</sup> As shown in Figure 5, a more complicated behavior is observed. The lattice parameters reported here for the high-temperature compounds  $\text{LaFe}_4\text{Sb}_{12}$ ,  $\text{CeFe}_4\text{Sb}_{12}$ , and  $\text{PrFe}_4\text{Sb}_{12}$  are consistent with previously reported values. From these first three compounds, there was no obvious contraction of the unit cell, which supports the model of the lanthanide fitting loosely in the iron–antimony framework. With the three new high-temperature skutterudites  $\text{NdFe}_4\text{Sb}_{12}$ ,  $\text{SmFe}_4\text{Sb}_{12}$ , and  $\text{GdFe}_4\text{Sb}_{12}$  reported here, it is clear that the unit cell does contract. The nonlinear nature of the contraction relative to the lanthanide ionic radius suggests a complicated behavior involving, for example, small rotations of the iron–antimony octahedra. The magnitude of the contraction, however, is much less than expected on the basis of changes in the ionic radii. This continues to support the model of the lanthanide cation fitting loosely in the iron–antimony framework.

The variation in the unit cell size of the low-temperature phases with the rare earth metal cation is surprisingly complicated. The unit cell size decreases monotonically with decreasing ionic radius from lanthanum through gadolinium and then increases with decreasing ionic radius from terbium through lutetium. This indicates that there may be a structural difference between the early and late rare earth elements. Europium and

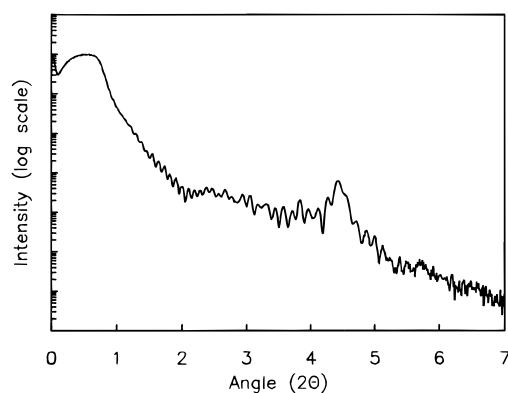


**Figure 6.** Low-angle X-ray diffraction of the thick Lu–Fe–Sb multilayer used for structural analysis. The multilayer peak corresponds to a repeat length of 21 Å. The total film thickness is 906 Å.

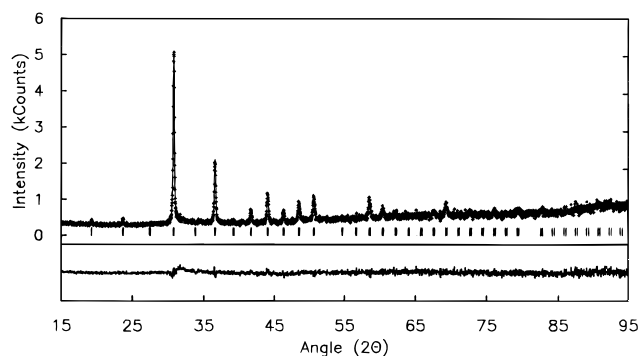


**Figure 7.** Results of the refinement of  $\text{Lu}_{1-x}\text{Fe}_4\text{Sb}_{12}$ . Space group:  $m\bar{3}$ .  $a = 9.1921(2)$  Å.  $R_{\text{wp}} = 8.9$  Atomic positions: Lu,  $16f$  ( $x = 0.048(8)$ , occupancy = 0.65(8)); Fe, 8c; Sb, 24g ( $y = 0.3341(6)$ ,  $z = 0.1592(5)$ ). Errors for least significant digits are given in parentheses. Data are shown as crosses; the line is the refined pattern. The difference plot is shown underneath on the same scale.

ytterbium stand out from the observed trend in unit cell size. This is because these elements are divalent as a result of the near half-filling or filling of the 4f shell. The observed lattice parameters of the europium and ytterbium compounds are consistent with this interpretation.  $\text{Eu}^{2+}$  is slightly larger than  $\text{La}^{3+}$ , and the europium-containing low-temperature skutterudite is slightly larger than the lanthanum-containing compound.  $\text{Yb}^{2+}$  is similar in size to  $\text{Gd}^{3+}$ , and the respective skutterudites have similar lattice parameters.

To search for a potential structural difference between the early and late rare earth elements, a Lu–Fe–Sb multilayer was prepared which was designed to allow structure refinement by the Reitveld procedure. The multilayer was directly deposited on an off-cut, single-crystal quartz substrate. The substrate was off-cut to provide a uniform, featureless background for the diffraction experiment. Low-angle X-ray diffraction, shown in Figure 6, was used to measure the film thickness (900 Å) so an accurate absorption correction could be applied to the Reitveld refinement. Care was taken to ensure that the incident beam did not extend beyond the edges of the sample at the lowest angle in the scan and that the detector field of view contained the entire illuminated area of the sample.

The data are shown in Figure 7. The film thickness is a small fraction of the penetration depth of the X-ray beam, so there is a large fluorescent background from the substrate which increases as a function of the angle. It is comparable to the peak intensities near 65° and completely obscures the diffraction between 85 and 95°. The refinement program (DBWS-

(17) Shelton, R. N.; McCallum, R. W.; Adrian, H. *Phys. Lett. A* **1976**, *56*, 213.

90086PC<sup>18</sup>) overestimates the background intensity and underestimates the peak intensity in this region. This results in a systematic error in the refined thermal parameters, despite the accurate absorption correction used. However, it was still possible to obtain useful information about atomic positions from these data.

The structure was initially refined in the same space group and with the same atomic positions as the analogous LaFe<sub>4</sub>Sb<sub>12</sub> compound (*Im* $\bar{3}$ ). It was possible to refine this structure to residuals of  $R_{wp} = 8.9$  and  $R^2 = 24$ . The occupancy of the lutetium was found to be 65%, close to that of the starting composition, in contrast to the full occupancy of the high-temperature compounds. The isotropic thermal parameter of the lutetium atom was anomalously large compared with those of the other atoms in the structure. However, the fit could be improved slightly, and the refined thermal parameter of the lutetium reduced, by allowing the lutetium to be randomly displaced by 0.7 Å along one of the eight possible body diagonal directions, occupying the 16*f* rather than the 2*a* Wyckoff site. This static displacement moves the lutetium toward a triangular face of antimony atoms and therefore increases the bonding of the lutetium to the iron–antimony framework. This distortion may explain the observed discontinuity in the unit cell size as a function of rare earth element cation. It is likely that the Tb, Dy, Ho, Er, Tm, and Lu low-temperature skutterudites all show the same random displacement of the rare earth element.

### Conclusion

We have demonstrated that it is possible to produce metastable, filled skutterudites with all the lanthanides using the multilayer precursor method. These metastable skutterudites have a partial occupancy of the lanthanide site, resulting in a deficiency of bonding electrons and an expanded unit cell. The formation of the iron–antimony framework controls the nucleation kinetics, and therefore it should be possible to include

any electropositive element in the lanthanum site of the La<sub>1-x</sub>Fe<sub>4</sub>Sb<sub>12</sub> structure. For cations with an ionic radius smaller than that of gadolinium (0.94 Å), the ion is displaced from the center of its interstitial site, which opens the possibility of ferroelectricity in these materials.

From these results, it is possible to point to a number of research directions for seeking improved thermoelectric materials. The disorder on the cation site is credited with reducing the phonon thermal conductivity. However, it is not obvious whether the static disorder of the late rare earth elements or the dynamic disorder of the early rare earth elements would be superior in this regard. In addition, the partial occupancy of the metastable compounds presents an opportunity to tune the electronic properties by controlling that occupancy. However, it will first be necessary to demonstrate that the occupancy can be controlled synthetically. These compounds also show a large variation in unit cell dimensions, which can be used to modify the band structure and therefore optimize the thermopower. The thin-film geometry of the films produced is ideal for measurement of the electrical conductivity and Seebeck coefficient. While techniques to measure thermal conductivity on thin-film samples have been developed,<sup>19,20</sup> bulk measurements on bar samples would be the most accepted measurement technique. With the deposition rates and equipment used in this study, a 300 mg sample would require approximately 10 h of deposition time and produce sufficient material for hot pressing a suitable bar specimen. Finally, the insensitivity of the synthesis to the particular cation used suggests that these metastable materials can be made with any electropositive element in that position. This provides a wide range of possible compounds to test for optimal thermoelectric properties. Such a search is now possible because the multilayer precursor method allows the rapid synthesis of large families of related metastable compounds.

IC9702375

(18) A. Sakhivel and R. A. Young, School of Physics, Georgia Institute of Technology, Atlanta, GA 30332.

(19) Cahill, D. G.; Katiyar, M.; Abelson, J. R. *Phys. Rev. B* **1994**, *50*, 6077.

(20) Cahill, D. G. *Rev. Sci. Instrum.* **1990**, *61*, 802.